Nuclear Engineering and Technology 51 (2019) 1983–1990

Contents lists available at ScienceDirect

Nuclear Engineering and Technology

journal homepage: www.elsevier.com/locate/net

Original Article

200 MeV Ag^{15+} ion beam irradiation induced modifications in spray deposited MoO_3 thin films by fluence variation

R. Rathika [a], M. Kovendhan [b, *], D. Paul Joseph [c], K. Vijayarangamuthu [d], A. Sendil Kumar [e], C. Venkateswaran [f], K. Asokan [g], S. Johnson Jeyakumar [a, **]

[a] Department of Physics, TBML College, Porayar, 609307, India
[b] Department of Environmental Engineering, Inha University, Incheon, 22212, South Korea
[c] Department of Physics, National Institute of Technology, Warangal, 506004, India
[d] Center for Nanoscience and Technology, Pondicherry University, Pondicherry, 605014, India
[e] Department of Physics, KL Education Foundation, Vaddeswaram, Guntur District, Andhra Pradesh, 522502, India
[f] Department of Nuclear Physics, University of Madras, Guindy Campus, Chennai, 600025, India
[g] Inter University Accelerator Centre, Aruna Asaf Ali Marg, New Delhi, 110067, India

ARTICLE INFO

Article history:
Received 10 February 2019
Received in revised form
23 May 2019
Accepted 3 June 2019
Available online 3 June 2019

Keywords:
Ion beam technology
MoO_3 thin films
Spray coatings
Optical materials and properties
Radiation damage

ABSTRACT

Spray deposited Molybdenum trioxide (MoO_3) thin film of thickness nearly 379 nm were irradiated with 200 MeV Ag^{15+} ion beam at different fluences (Ø) of 5×10^{11}, 1×10^{12}, 5×10^{12} and 1×10^{13} ions/cm^2. The X-ray diffraction (XRD) pattern of the pristine film confirms orthorhombic structure and the crystallinity decreased after irradiation with the fluence of 5×10^{11} ions/cm^2 due to irradiation induced defects and became amorphous at higher fluence. In pristine film, Raman modes at 665, 820, 996 cm^{-1} belong to Mo–O stretching, 286 cm^{-1} belong to Mo–O bending mode and those below 200 cm^{-1} are associated with lattice modes. Raman peak intensities decreased upon irradiation and vanished completely for the ion fluence of 5×10^{12} ions/cm^2. The percentage of optical transmittance of pristine film was nearly 40%, while for irradiated films it decreased significantly. Red shift was observed for both the direct and indirect band gaps. The pristine film surface had densely packed rod like structures with relatively less porosity. Surface roughness decreased significantly after irradiation. The electrical transport properties were also studied for both the pristine and irradiated films by Hall effect. The results are discussed.

1. Introduction

Molybdenum trioxide (MoO_3) is a transition metal oxide with excellent optical and electrical properties and is a high-performance cathode material. The MoO_3 has a variety of polymorphs with different structural configurations such as α-MoO_3, β-MoO_3, ε-MoO_3 and h-MoO_3 [1]. MoO_3 is also chemically, thermodynamically stable material and is a potential candidate for diverse range of applications in optical memories, gas sensors, lithium batteries, solar cells and electrochromic devices [2–5]. Uranium-molybdenum alloy with higher molybdenum content having interesting properties is a potential candidate for fuel production in nuclear reactors [6]. The Zr-alloy coated Mo-alloy cladding meet the thermal and mechanical requirements for normal operation of nuclear reactors by controlling heat produced due to nuclear decay and thereby reducing the damage of the reactor core [7]. In recent years, many researchers are investigating MoO_3 material because of the fact that it possesses photochromic, gasochromic and electrochromic properties, which makes it as a suitable compound for optoelectronic device fabrication.

The MoO_3 thin film can be prepared by different methods including sputtering [8,9], electron beam evaporation [10], sol–gel [11,12], spray deposition [13–15], pulsed laser deposition [16,17] and thermal evaporation [18,19]. Among these, spray pyrolysis is an effective method used to deposit metal oxides in particular MoO_3 the thin film whose properties depend on spraying

* Corresponding author.
** Corresponding author.
E-mail addresses: mail2rathiga@gmail.com (R. Rathika), mkovendhan@gmail.com (M. Kovendhan), palphymail@gmail.com (D.P. Joseph), vrmuthu@gmail.com (K. Vijayarangamuthu), sendilphy@gmail.com (A.S. Kumar), cvenkateswaran@gmail.com (C. Venkateswaran), asokan42@gmail.com (K. Asokan), drsjohnson@rediffmail.com (S.J. Jeyakumar).

https://doi.org/10.1016/j.net.2019.06.004

parameters that can be easily tuned during film deposition. The instrumental set-up of spray pyrolysis technique is simple and cost effective. S.A. Khalate et al., studied the effect of different substrate temperatures on properties of spray deposited α-MoO_3 [20]. Electro synthesized α-MoO_3 shows enhanced electrochromic property after annealing at a temperature of 450 °C [21]. Mahajan et al. observed an increase in coloration efficiency of spray deposited MoO_3 thin film from 10% to 19% [5].

Improvement in the properties of existing materials could be achieved using different deposition techniques or tuning their properties to suit the needs of technological applications. The swift heavy ion (SHI) irradiation is a useful tool to modify material properties by introducing various type of defects like point defects, cluster defects, phase transformation along the ion track due to electronic excitation, depending on projectile ion and target material [22]. In our past work we have investigated modifications in properties of WO_3 thin films because of swift heavy ion irradiation [23]. Optical absorption of electron-beam evaporated MoO_3 films increased after irradiation with 2 MeV N^+ ion [24].

The property modification and band gap tuning of materials by swift heavy ion beam irradiation may lead to better performance of the material in various optoelectronic device applications [25–27]. To our knowledge, no reports are available on MoO_3 films irradiated with silver ion. Irradiation induced modifications in MoO_3 may significantly improve the properties for its effective usage in a variety of applications. This motivated us to investigate the effect of 200 MeV Ag^{15+} ion beam irradiation on properties of spray deposited MoO_3 thin films with various ion fluences ranging from 5×10^{11} to 1×10^{13} ions/cm^2.

2. Experimental procedure

2.1. Spray deposition

The stoichiometric amount of $MoCl_5$ is dissolved in a 300 ml of bidistilled water and 2 ml of hydrochloric acid is added to avoid precipitation. The prepared precursor solution was then sprayed onto ITO coated glass substrate maintained at 325 °C. The detailed procedure of the spray pyrolysis instrumental setup for thin film deposition is described elsewhere [28]. Pyrolytic decomposition takes place on the surface of the heated substrate and MoO_3 thin film is formed by volmer weber growth mode. In general, the thin film growth modes are classified as Frank-Vander Merwe growth (layer by layer), Volmer-Weber growth (island mode), Stranski Krastanov growth (layer and island mixed growth mode) [29]. Among these, the spray pyrolysis method always follows the Volmer-Weber growth (island mode). Upon spraying the precursor aerosol, tiny three-dimensional nuclei are formed randomly all over the substrate without complete surface coverage. With subsequent spraying and due to the substrate temperature, the islands gradually coalesce with each other forming a continuous oxide film by filling the entire surface of the substrate with high density of grain boundaries between the crystallites [30]. The spray parameters were optimized to ensure that the quality of obtained film was good and attach/bond well onto the substrate.

2.2. Irradiation experiments

Spray deposited film of area 0.5 × 1 cm^2 and thickness nearly 379 nm were then irradiated with 200 MeV Ag^{15+} ions at various fluences of 5×10^{11}, 1×10^{12}, 5×10^{12} and 1×10^{13} ions/cm^2. Swift heavy ions were accelerated using particle accelerator to very high energy (in MeV range), so that they have enough energy to penetrate into the solid material. We have used 15 UD Pelletron accelerator available at Inter university accelerator centre, (IUAC) New Delhi for the material modification. Irradiation parameters for these samples such as energy, fluence, incident angle, etc. were estimated using Stopping Range of Ions in Matter (SRIM) program prior to irradiation [31].

The Ag^{15+} ion beam transfers an energy of 2023 eV/Å by electronic energy loss due to inelastic collisions and 5.569 eV/Å by nuclear energy loss through elastic collisions, as simulated from SRIM (Fig. 1(a)). The calculated projected range of Ag^{15+} ion and S_e/S_n ratio values are 15.12 μm and 363 respectively in the MoO_3 lattice. This makes sure that the electronic energy loss is more dominating through which the Ag^{15+} ions deposit their energy onto the MoO_3 lattice and prevent ions getting implanted into the material.

2.3. Characterization methods

Various characterization techniques were used to investigate both the pristine and the irradiated samples. Structural analysis of MoO_3 thin films were carried out using X'pert High scorer,

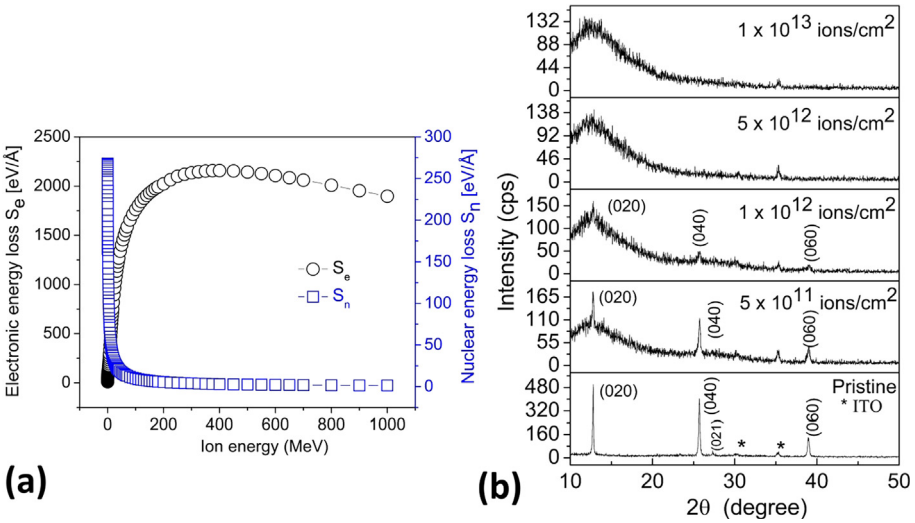

Fig. 1. (a) Nuclear and electronic energy losses for various incident energies, (b) XRD patterns of pristine and 200 MeV Ag^{15+} ion beam irradiated MoO_3 thin films at various fluences.

PANalytical X-ray diffractometer with CuK_α radiation in powder diffraction mode in Bragg-Brentano geometry. Raman spectra obtained from Renishaw system in back scattering geometry at an excitation wavelength of 514.5 nm with an argon ion laser source. The optical transmittance properties were studied by UV-Vis double beam spectrometer with JASCO type V-570 in normal incidence mode. The AFM (SPI 3800 N) was utilized in non-contact mode to investigate surface topography. To measure film thickness XP-1 surface profiler from Ambios Technology Inc. was used. Electrical transport properties were measured at room temperature using the Ecopia HMS 3000 Hall measurement system.

3. Results and discussions

3.1. X-ray diffraction (XRD) analysis

Fig. 1(b) shows the XRD patterns of pristine and irradiated MoO_3 thin films at various fluences 5×10^{11}, 1×10^{12}, 5×10^{12} and 1×10^{13} ions/cm^2. The observed pattern matches well with the standard XRD pattern for orthorhombic structure (JCPDS No.: 76–1003) [32]. Bouzidi et al., synthesized MoO_3 thin film with orthorhombic structure above 250 °C [13]. MoO_3 thin films prepared by Boudaoud et al., using the spray pyrolysis method also showed orthorhombic symmetry [33]. The XRD spectra of the pristine film show high intense (020), (040), (060) peaks and a less intense (021) peak. The absence of secondary phase and impurities clearly reveals that the obtained sample is single phase with polycrystalline nature. The texture coefficient [34] calculated using the following equation show preferred growth along (020) and (040) planes.

$$\text{Texture coefficient } TC_{hkl} = \frac{I_{hkl}/I_{0hkl}}{\frac{1}{N}\sum_{N=1}^{N} I_{hkl}/I_{0hkl}} \quad (1)$$

where, I_{hkl} is the intensity obtained for a particular ($h\ k\ l$) plane, I_{0hkl} is the standard intensity of the same ($h\ k\ l$) plane from the JCPDS database, and N is the total number of XRD reflections observed in the diffraction pattern. Higher value of TC_{hkl} represents greater preferred growth along that plane.

Structural parameters such as crystallite size (D), dislocation density (δ), the number of crystallites per unit surface area (N) and micro strain (ε) were estimated using the equations given below [35],

$$D = \frac{0.9\lambda}{\beta \cos\theta} \quad (2)$$

$$\delta = \frac{1}{D^2} \quad (3)$$

$$N = \frac{d}{D^2} \quad (4)$$

$$\varepsilon = \frac{\beta \cos\theta}{4} \quad (5)$$

where d is film thickness, λ is the wavelength of X-ray (1.5406 Å), θ is Bragg angle, and β is FWHM in radians. The corresponding values for pristine and irradiated samples are reported in Table 1. From the results it is clearly seen that the micro strain, dislocation density and number of crystallites per unit area increased after ion irradiation. The microstrain value increased due to reduced crystallinity and increase in tensile stress [36]. Plastic deformation that takes place during irradiation generates dislocations. Grain boundaries restrict expansion of dislocations which in turn is related to grain size. It is clear that grain size decreased significantly after irradiation. As grain size reduces density of grain boundaries increase. Hence, smaller grain size suggests higher density of smaller sized dislocations [37]. Grain splitting occurring during irradiation was the main reason for an increase in number of crystallites per unit area, and it is explained briefly in the AFM section.

Williamson-Hall plot (Fig. 2(a)) was also plotted for the pristine sample to confirm the crystallite size of deposited MoO_3 film. By linear fitting, the average values of crystallite size and micro strain was found to be 74 nm and 0.00059 from y intercept and slope of fitted line respectively [38]. Upon irradiation, intensity of the diffraction peak begins to decrease while peak width increases. At fluence 5×10^{11} and 1×10^{12} ions/cm^2, persistence of weak XRD peaks indicate partially amorphized MoO_3 film. The reduced peak intensity was a consequence of point defects induced by SHI irradiation [35]. It is observed that (040) peak is radiation resistant to the ion beam at low fluence [39]. Partial amorphization of material is attributed to the very high localized temperature created by Ag ion in MoO_3 [40,41]. When lattice temperature increases above threshold value of electronic stopping, a cylindrical region around ion track got damaged forming latent tracks of the modified material. At lower fluence, the latent tracks by passage of ion beam through lattice are separated from each other with some space hence amorphization does not takes place at lower fluence. As fluence increases, the latent tracks begin to overlap with each other and above 1×10^{12} ions/cm^2 fluence nearly all the tracks overlap resulting in complete lattice damage leading to amorphization of MoO_3 thin film [42,43]. At higher fluence, above 1×10^{12} ions/cm^2, the XRD peaks vanished and the film became completely amorphous.

Table 1
Structural parameters of the pristine and irradiated MoO_3 thin films.

Fluence (ions/cm^2)	Plane	Average crystallite size D (nm)	Dislocation density δ (x10^{16} m^{-2})	Micro strain ε	Number of particles unit area N (x10^7/nm^{-2})
Pristine	(020)		0.019	0.0004	07.6
	(040)	55.8	0.037	0.0006	14.9
	(060)		0.051	0.0007	20.6
5×10^{11}	(020)		0.052	0.0007	21.3
	(040)	36.6	0.080	0.0009	32.5
	(060)		0.103	0.0011	41.9
1×10^{12}	(020)		0.091	0.0010	37.2
	(040)	33.4	0.185	0.0014	75.1
	(060)		0.051	0.0007	20.8

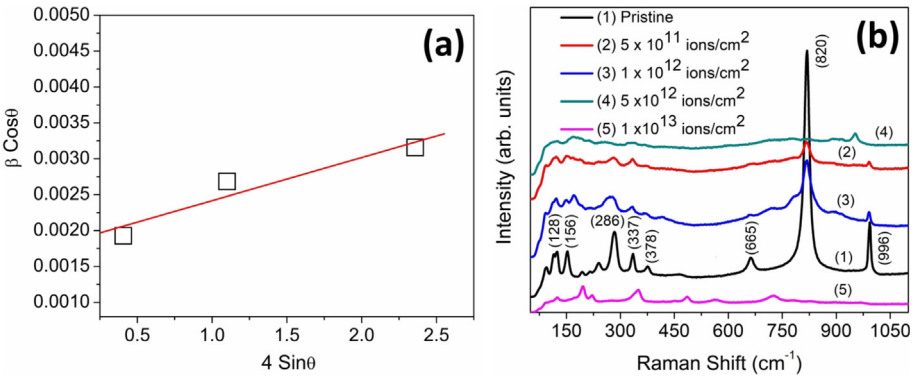

Fig. 2. (a) Williamson-Hall plot of pristine MoO_3 thin film, (b) Raman spectra of pristine and irradiated MoO_3 thin films at various fluences.

3.2. Raman spectra

Raman spectroscopic investigation has been used to analyze the local structural variations in MoO_3 thin film. Fig. 2(b) shows the modification induced in irradiated samples with irradiation fluence of $5 \times 10^{11}, 1 \times 10^{12}, 5 \times 10^{12}$ and 1×10^{13} ions/cm^2 compared to the pristine film. The structure of α-MoO_3 belongs to Pbnm space group with standard lattice parameters: a = 3.9628 Å, b = 13.855 Å and c = 3.6964 Å (JCPDS No.: 76–1003). The MoO_3 stoichiometry is formed from the double layer of corner shared MoO_6 octahedral stacked along the (010) plane [44].

The Raman peaks around 1000-600 cm^{-1} belongs to Mo–O stretching vibrations [4]. The peak at 996 cm^{-1} arised from M = O short terminal bond of unshared oxygen which is the characteristic peak of α-MoO_3 [45]. The observed orthorhombic structure corroborates well with XRD results. The sharp intense peak at 820 cm^{-1} arise from the O–Mo_2 bridging bond of corner shared oxygen [46]. The peak at 665 cm^{-1} (O–Mo_3) is from edge shared oxygen [47]. Raman active modes at 337, 373, 286 cm^{-1} (400-200 cm^{-1}) were assigned to the Mo–O bending mode [48]. In low frequency range 128 and 156 cm^{-1} Raman-active lattice mode are also observed which are less significant [47,49].

It can be seen that intensity of Raman peaks decreased significantly upon irradiation with fluence 5×10^{11} ions/cm^2. The incident silver ion created oxygen vacancies by displacement of oxygen atoms from its lattice site to interstitial site [50]. Both the XRD and Raman results show degradation in crystallinity which indicates creation of point defects by irradiation. According to thermal spike model, the material along the ion beam track get melted due to high energy deposition and aids diffusion to take place. Generally, diffusion cause swelling, creeping in amorphous material and phase separation in the case of alloys. However, in crystalline metals and semiconductors, diffusive atom transport is usually proceeded by creation of point defects that provides space for movement of atoms. Observed degradation in crystallinity is attributed to irradiation induced Frenkel defects that constitute oxygen vacancy and an interstitial pair. Amount of defects increased and thus peak intensity decreased with an increase in fluence [51]. Literature also support creation of point defects by irradiation in metal oxides mostly to be Frenkel defects [52].

For fluences 5×10^{11} and 1×10^{12} ions/cm^2 only few weak peaks remained due to partial amorphization, which corroborate with the XRD results [35]. The sample irradiated with fluence 5×10^{12} ions/cm^2 undergo much more damage compared to other two lower fluences 5×10^{11} and 1×10^{12} ions/cm^2. Consequently, the Raman modes vanished and the film became completely amorphous at higher fluences.

3.3. Optical investigation

Transmittance spectra (Fig. 3(a)) shows modifications in optical properties after irradiation with different fluences. The pristine film exhibits a high transparency in NIR range while in the visible region it was around 10%. Previous research findings reveal, transmittance decreases and absorption edge shift towards the higher wavelength with increase in substrate temperature [10,13]. Therefore, high substrate temperature (325 °C) used during film deposition accounts for this observed low transmittance in the pristine film. The absorption edge is observed at 450 nm for pristine film and it shifted towards higher wavelength after irradiation. This shift

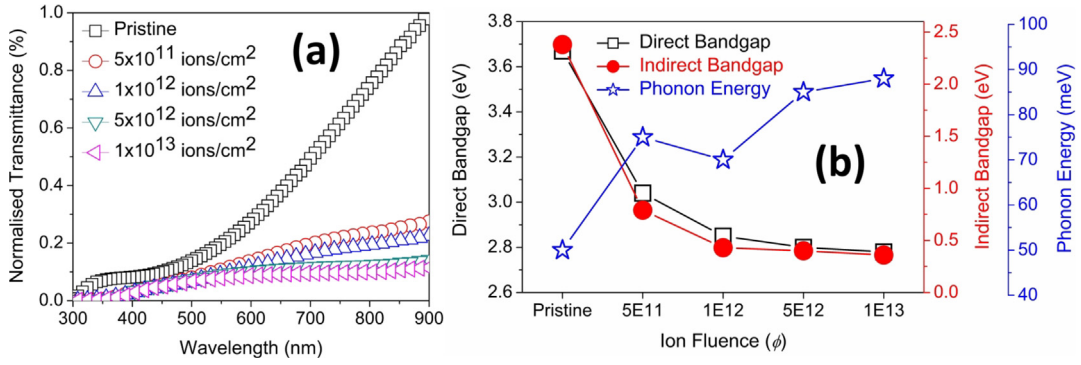

Fig. 3. (a) Optical transmittance spectra and (b) variation of the direct bandgap, indirect bandgap and phonon energy of pristine and irradiated MoO_3 thin films at various fluences.

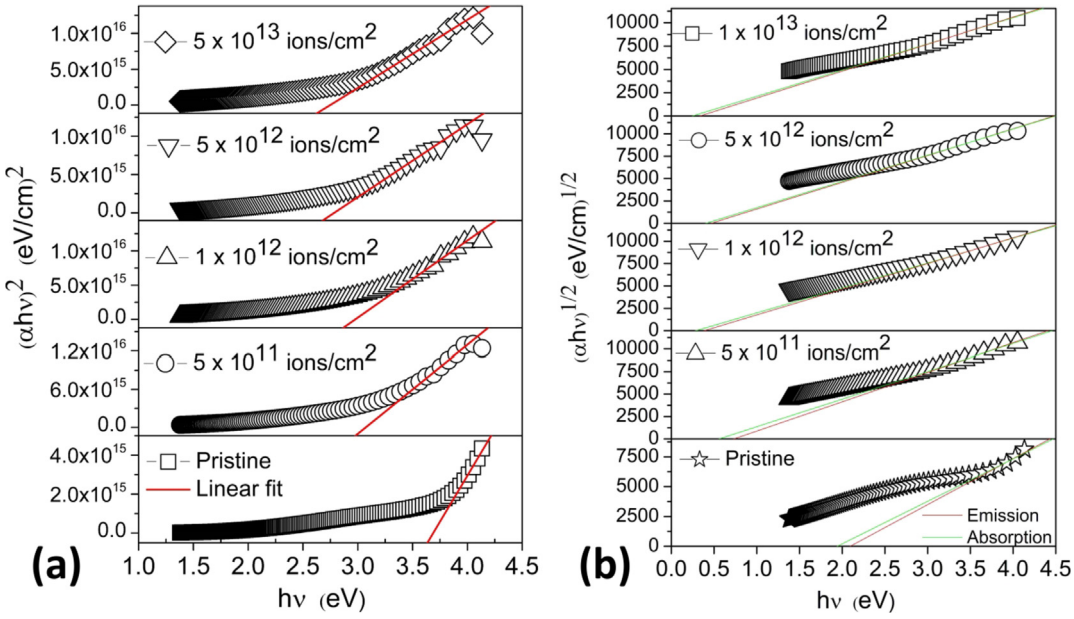

Fig. 4. (a) Estimation of the direct band gap and (b) indirect band gap of pristine and irradiated MoO_3 thin films at various fluences.

indicates the decrease in optical band gap after irradiation.

From Beer Lambert's law [53],

$$I = I_0 \exp(-\alpha t) \quad (6)$$

Where I is the incident intensity, I_0 is the transmitted intensity.

The absorption coefficient (α) is given by

$$\alpha = \left(\frac{1}{d}\right) ln\left(\frac{1}{T}\right) \quad (7)$$

where T represents transmittance and d represents the film thickness.

From transmittance spectra, we observed consistent fall in optical transmittance with an increase in ion fluences [51]. This might be due to the reduced crystallinity and decrease in crystallite size, as observed in XRD pattern. Absorption coefficient increased with higher fluence and as a result strong optical absorption by material observed after irradiation [54]. Reasons behind the reduction in transparency by SHI irradiation could be better understood in following discussion. Many factors affect the optical transparency of MoO_3 film by the irradiation process. Irradiation induced distortions in the MoO_6 octahedral symmetry could cause variations in transmittance [55]. As fluence increases, more number of electrons get excited and move from valence band to conduction band thereby enhanced the light absorption [56,57]. From the XRD spectra, one can observe the reduction in crystallinity with ion fluence (Table 1) due to formation of defects and increased density of grain boundaries which act as scattering centers and reduce the optical transparency of the irradiated samples [41].

3.3.1. Optical bandgap estimation

The direct band gap values (E_g) has been estimated (Fig. 4(a)) by extrapolation of the best linear fit to the Tauc plot of $(\alpha h\nu)^2$ vs photon $h\nu$ to the energy axis at $\alpha = 0$. Expression for allowed direct and indirect transitions [55,58] is,

$$\alpha h\nu = A(h\nu - E_g)^n \quad (8)$$

where, α-absorption coefficient, A - optical constants for indirect and direct transitions, h - Planck's constant, ν - frequency, E_g-band gap energy.

From Tauc plot of $(\alpha h\nu)^{1/2}$ vs $h\nu$ (Fig. 4(b)), indirect band gap values (E_{gind}) were estimated by linear fitting. Phonon energies were also estimated by solving two simultaneous equations from absorption fit and emission fit for indirect transitions [59]. Optical band gap values and the corresponding phonon energy values of pristine and irradiated samples for various fluences are given in Table 2. The direct band and the indirect band gap of pristine MoO_3 film were found to be 3.67 and 2.38 eV respectively, which was higher than those reported in previous works [10,13].

Upon irradiation, both direct band gap and indirect band gap values systematically reduced in comparison with pristine one and thus the red shift observed in both the cases. The optical band gap values decreased (Fig. 3(b)) consistently with increased fluence and phonon energy increased correspondingly [23,50,60]. The SHI irradiation induced extra shallow levels into the forbidden band

Table 2
Calculated optical band gaps and phonon energy of pristine and irradiated MoO_3 thin films.

Fluence (ions/cm^2)	Direct band gap E_g (eV)	Indirect band gap E_{gind} (eV)	Phonon energy E_p (meV)
Pristine	3.67	2.38	50
5×10^{11}	3.04	0.79	75
1×10^{12}	2.85	0.43	70
5×10^{12}	2.80	0.40	85
1×10^{13}	2.78	0.36	88

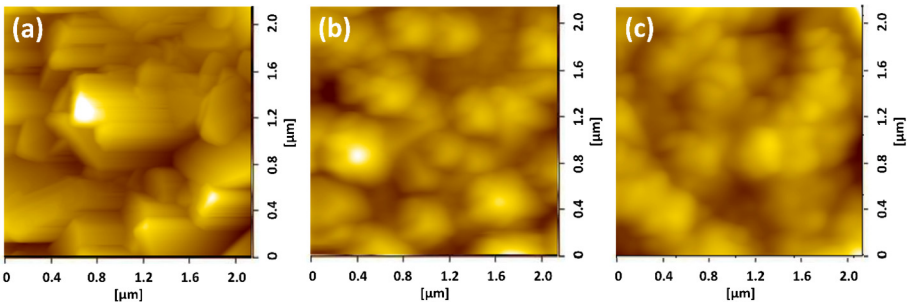

Fig. 5. The 2D AFM images of (a) the pristine MoO_3 thin film and those of irradiated with (b) 5×10^{11} ions/cm^2, (c) 1×10^{13} ions/cm^2.

Table 3
Average surface roughness and grain size of the pristine and irradiated MoO_3 thin films from AFM measurements.

Fluence (ions/cm^2)	Average surface roughness (R_{rms}) (nm)	Average grain size (nm)
Pristine	4.96	42
5×10^{11}	2.82	34
1×10^{13}	2.23	23

gap and density of localized states increased as a function of fluence [61]. The conduction band consist of lone pair orbitals, whereas the valence band is formed by the antibonding orbitals. 200 MeV silver ions excite the lone pair electrons of the valence band to its higher energy level. Vacancies created were instantly filled by the outer bonding electrons which in turn generated more holes. This Auger process, leading to a vacancy cascade induced electronic structure modification [62] thereby improvement in probability of inter-band transition. The observed reduction in the band gap value is ascribed to this tailing effect of the valence band, due to irradiation [37,63]. The variation in direct bandgap, indirect bandgap and phonon values at various ion fluences are clearly seen in Fig. 3(b).

3.4. Atomic force microscopy

The AFM measurement was carried out in non-contact mode to analyze the surface topography. Fig. 5 shows the 2D surface microstructure of the (a) pristine and irradiated films with fluence (b) 5×10^{11} and (c) 1×10^{13} ions/cm^2. The surface of the pristine film was found to have densely packed rod like structures and distribution was symmetric over the surface. Previously published work suggest the MoO_3 film usually exhibit nanorod like structure [64–66]. The root means square surface roughness (R_{rms}) calculated using equation (8) and average grain size of the pristine and irradiated films from the respective AFM images were estimated.

$$R_{rms} = \frac{1}{N}\left[\sum_{i=1}^{N}\left(Z^i - \overline{Z}\right)^2\right]^{\frac{1}{2}} \quad (9)$$

where N is the number of surface height data and $\overline{Z}$ is the mean height distance [67].

Generally, the spray deposited films have a rough surface due to island growth mode with spike like features. The SHI beam irradiation reduces the surface roughness significantly. It was observed that the surface of irradiated samples was comparatively smoother than that of the pristine one (Table 3) [68]. As swift heavy ion beam penetrates the target material, roughening and smoothening effect compete with each other on the surface of the materials [69]. Irradiation induced heat is transferred from electronic sub-system to ionic sub-system. Heated up track caused a local melting of surface material along the ion path [70]. Viscous flow of molten material was the basic mechanism behind this occurrence of smoothening reaction on the surface [71]. The R_{rms} decreased with increase in fluence and minimum value is observed for maximum fluence of 1×10^{13} ions/cm^2 [51]. These analyses were in good agreement with partial amorphization observed in XRD and Raman results. The grain size of pristine film was 922 nm, whereas it was 714 nm and 288 nm for fluences 5×10^{11} and 1×10^{13} ions/cm^2 respectively. These results suggested that a decrease in average grain size upon irradiation, depend on ion fluence. The grain fragmentation takes place after irradiation, leading to such grain size reduction.

An enormous heat transferred momentarily to the lattice during 'Ag' ion passage which leaves ion track under localized high pressure. Due to this high energy dissipated in a short interval of time, it has created lattice vibrations and point defects. When fluence was higher compared to threshold value, grain splitting come into play, decreasing the grain size [72]. Further, with an increase in ion fluence more zones were subjected to high pressure so that additional grain splitting occurs. Accordingly, more grain size reduction observed at higher fluence than at lower fluence [36,73]. The AFM micrographs revealed the fluence dependent surface modification of MoO_3 film. Similar effects were observed for other fluences also which are not shown here.

Table 4
Transport parameters of pristine and irradiated MoO_3 thin films.

Fluence (ions/cm^2)	ρ (Ω cm)	σ (Ω cm)$^{-1}$	N_b (/cm^3)	μ (cm^2/Vs)
Pristine	1.530×10^{-3}	6.534×10^{2}	2.599×10^{19}	1.570×10^{2}
1×10^{12}	1.442×10^{-3}	6.934×10^{2}	3.342×10^{19}	1.295×10^{2}
5×10^{12}	1.229×10^{-2}	8.137×10^{1}	3.181×10^{18}	1.597×10^{2}
1×10^{13}	1.732×10^{-1}	5.775×10^{0}	1.255×10^{17}	2.874×10^{2}

3.5. Hall effect analysis

Table 4 summarize the Hall parameters like, resistivity, conductivity, carrier concentration and mobility measured at room temperature for MoO_3 thin films before and after irradiation. Irradiating the pristine MoO_3 film with Ag^{15+} ions of fluence 1×10^{13} ions/cm^2 increases the resistivity to 1.732×10^{-1} from 1.530×10^{-3} Ω cm. The resistivity is expected to decrease after irradiation due to decrease in bandgap, but the observed grain size

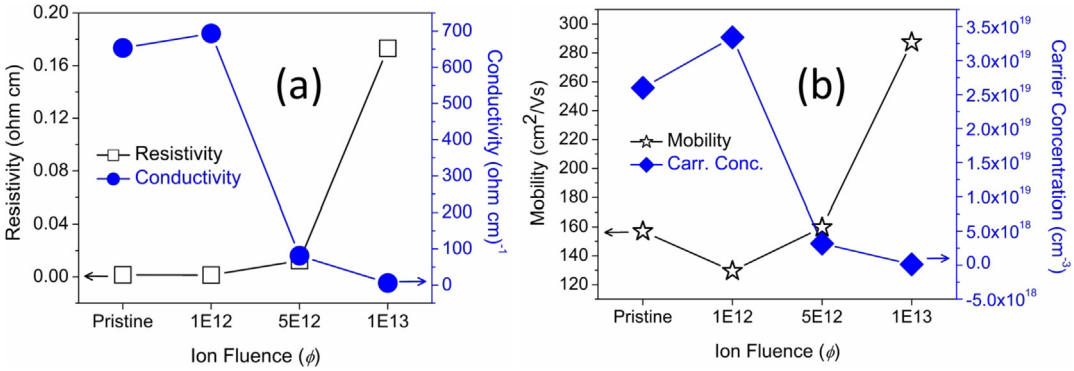

Fig. 6. (a) Variation of resistivity and conductivity and (b) Mobility and carrier concentration of the pristine and irradiated MoO_3 thin films at various fluences.

reduction primarily dominated this effect. Therefore, we could say that resistivity has increased by grain boundary scattering [74].

In general, grain boundaries are defects that scatter charge carriers, thereby increasing the resistivity. If grain size was bigger than the mean free path of charge carriers, influence of grain boundaries on resistivity would be negligible. This effect becomes more pronounced once the grain size reaches the carrier's mean free path values; further reducing the grain size would result in a considerable increase in resistivity [75]. The scattering of charge carriers becomes dominant due to higher density of grain boundaries. The dependence of electrical resistance on the grain size was already well established by Mayadas-Shatskes model [51,76]. Therefore, smaller grains result in higher density of defects that increased the resistivity. When grain size is comparable to the carrier mean free path, the transported charge carriers undergo scattering by the grain boundaries which possesses significant amount of defects. As a result, the amount of charge carriers participating in conduction process is reduced leading to decrease in conductivity.

The variation of resistivity and conductivity with ion fluence is depicted in Fig. 6(a). The value of resistivity was found to increase with increasing fluence and the highest value was observed for maximum fluence [51,77]. In general, stoichiometric MoO_3 behaves as an insulator. In our case, the deposited film is sub-stoichiometric (MoO_3-x) with oxygen vacancies and extra molybdenum atoms which serve as donors that influence the electrical properties. The semiconducting type also depend on the position of Fermi level, if the Fermi level is near the valence band it may lead to p-type. It is also reported that the electrical conductivity in MoO_3-x generally depends on occupancy of d-level [44]**.** Oxygen vacancies are also reported to create additional 4d levels forming below the Fermi level, which may favour hole transport [78]**.** In addition, at higher fluence, localized recrystallization [79,80] might have resulted leading to compensation of defects and free carriers which apparently leads to a reduced carrier concentration behaviour as seen in the plot of mobility and carrier concentration as a function of ion fluence in Fig. 6(b).

4. Conclusion

In summary, we have investigated the influence of 200 MeV Ag^{15+} swift heavy ion beam irradiation on MoO_3 thin films in the fluence range from 5×10^{11} to 1×10^{13} ions/cm^2. The structural analysis by XRD and Raman techniques showed that both pristine and irradiated films to have orthorhombic structure. The increase in irradiation induced defects, reduced the crystallinity up to 1×10^{12} ions/cm^2 and films are amorphized at higher fluences. The optical transmittance reduced systematically as a function of ion fluence which is correlated to variation in grain size and defect creation. A significant variation in optical property achieved using irradiation suggests that one can tune it appropriately as per application requirements. Direct and the indirect band gap estimated from transmittance data showed red shift. It is observed that bandgap reduced drastically due to the formation of extra defect levels. Ion beam irradiation thus turns MoO_3 into a versatile compound by band gap tuning suitable for various applications. The AFM analysis indicates a morphological evolution at various fluences and surface smoothening of the irradiated films. Grain fragmentation eventually leads to the reduced grain size with the increase in ion fluence. The Hall effect study demonstrates a decrease in carrier concentration and increase in resistivity due to enhanced grain boundary scattering after irradiation. This study shows that the SHI irradiation causes remarkable change in the properties of MoO_3 thin films and induced modifications that are fluence dependent.

Acknowledgements

The authors thank the Inter University Accelerator Centre (IUAC), New Delhi, for providing access to the irradiation facility.

References

[1] L. Mai, F. Yang, Y. Zhao, X. Xu, L. Xu, B. Hu, Y. Luo, H. Liu, Mater. Today 14 (2011) 346–353.
[2] A.L. Pergament, V.P. Malinenko, L.A. Aleshina, E.L. Kazakova, N.A. Kuldin, J. Exp. Phys. 2014 (2014), 951297, 1–6.
[3] S.S. Sunu, E. Prabhu, V. Jayaraman, K.I. Gnanasekar, T.K. Seshagiri, T. Gnanasekaran, Sensor. Actuator. B 101 (2004) 161–174.
[4] B.S. Lee, Y. Kim, R. Deshpande, P.A. Parilla, E. Whitney, D.T. Gillaspie, K.M. Jones, A.H. Mahan, S. Zhang, A.C. Dillon, Adv. Mater. 20 (2008) 3627–3632.
[5] S.S. Mahajan, S.H. Mujawar, P.S. Shinde, A.I. Inamdar, P.S. Patil, Int. J. Electrochem. Sci. 3 (2008) 953–960.
[6] G.K. Suryaman, M.W. Wildan, S. Supardjo, Y.D. Agus Susanto, Urania J. Ilm, Daur Bahan Bakar Nukl 24 (2019) 135–142.
[7] B. Cheng, Y.J. Kim, P. Chou, Nucl. Eng. Technol. 48 (2016) 16–25.
[8] V. Nirupama, M. Chandra Sekhar, T.K. Subramanyam, S. Uthanna, J. Phys. Conf. Ser. 208 (2010) (012101)1–(012101)6.
[9] P.F. Carcia, E.M. McCarron, Thin Solid Films 155 (1987) 53–63.
[10] R. Sivakumar, R. Gopalakrishnan, M. Jayachandran, C. Sanjeeviraja, Curr. Appl. Phys. 7 (2007) 51–59.
[11] M. Dhanasankar, K.K. Purushothaman, G. Muralidharan, Appl. Surf. Sci. 257 (2011) 2074–2079.
[12] S.D. Gothe, A.A. Wali, D.S. Sutrave, Int. J. Eng. Res. Afr. 6 (2016) 26–32.
[13] A. Bouzidi, N. Benramdane, H. Tabet-Derraz, C. Mathieu, B. Khelifa, R. Desfeux, Mater. Sci. Eng. B 97 (2003) 5–8.
[14] N. Chaturvedi, S.K. Swami, V. Dutta, Sol. Energy 137 (2016) 379–384.
[15] B. Kannan, R. Pandeeswari, B.G. Jeyaprakash, Ceram. Int. 40 (2014) 5817–5823.
[16] C. Chang, J. Luo, T. Chen, K. Yeh, T. Huang, C. Hsu, W. Chao, C. Ke, P. Hsu, M. Wang, M. Wu, Thin Solid Films 519 (2010) 1552–1557.

[17] J.M. Camacho, A.I. Oliva, Thin Solid Films 515 (2006) 1881–1885.
[18] M.B. Rahmani, S.H. Keshmiri, J. Yu, A.Z. Sadek, L. Al-mashat, A. Moafi, K. Latham, Y.X. Li, W. Wlodarski, K. Kalantar-zadeh, Sensor. Actuator. B 145 (2010) 13–19.
[19] T.S. Sian, G.B. Reddy, J. Appl. Phys. 98 (2005) 98–101.
[20] S.A. Khalate, R.S. Kate, H.M. Pathan, R.J. Deokate, J. Solid State Electrochem. 21 (2017) 2737–2746.
[21] R.S. Patil, M.D. Uplane, P.S. Patil, Int. J. Electrochem. Sci. 3 (2008) 259–265.
[22] I.P. Jain, G. Agarwal, Surf. Sci. Rep. 66 (2011) 77–172.
[23] R. Rathika, M. Kovendhan, D.P. Joseph, A.S. Kumar, K. Vijayarangamuthu, C. Venkateswaran, K. Asokan, S. Johnson Jeyakumar, Nucl. Instrum. Methods Phys. Res. B 439 (2019) 51–58.
[24] R. Sivakumar, R. Sanjeeviraja, C. Jayachandran, M. Gopalakrishnan, S.N. Sarangi, D. Paramanik, T. Som, J. Appl. Phys. 101 (2007), 034913 (1–5).
[25] P. Mallick, C. Rath, J. Prakash, D.K. Mishra, R.J. Choudhary, D.M. Phase, A. Tripathi, D.K. Avasthi, D. Kanjilal, N.C. Mishra, Nucl. Instrum. Methods Phys. Res. B 268 (2010) 1613–1617.
[26] Y. Zhang, M.P.K. Sahoo, J. Wang, 19 (2017) 7032–7039.
[27] P. Sudhagar, K. Asokan, J.H. Jung, Y. Lee, S. Park, Y.S. Kang, 6 (2011) 1–7.
[28] M. Kovendhan, D.P. Joseph, E.S. Kumar, A. Sendilkumar, P. Manimuthu, S. Sambasivam, C. Venkateswaran, R. Mohan, Appl. Surf. Sci. 257 (2011) 8127–8133.
[29] E. Bauer, Z. Kristallogr. 110 (1958) 372–394.
[30] J.A. Venables, Introduction to Surface and Thin Film Processes, first ed., CAMBRIDGE UNIVERSITY PRESS, New York, 2003.
[31] www.srim.org.
[32] M. Kovendhan, D.P. Joseph, P. Manimuthu, S. Sambasivam, S.N. Karthick, K. Vijayarangamuthu, A. Sendilkuma, K. Asokan, H.J. Kim, B.C. Choi, C. Venkateswaran, R. Mohan, Appl. Surf. Sci. 284 (2013) 624–633.
[33] L. Boudaoud, N. Benramdane, R. Desfeux, B. Khelifa, C. Mathieu, Catal. Today 113 (2006) 230–234.
[34] M. Kovendhan, D. Paul Joseph, P. Manimuthu, A. Sendilkumar, S.N. Karthick, S. Sambasivam, K. Vijayarangamuthu, Hee Je Kim, Byung Chun Choi, K. Asokan, C. Venkateswaran, R. Mohan, Curr. Appl. Phys. 15 (2015) 622–631.
[35] A. Solanki, J. Shrivastava, S. Upadhyay, V. Sharma, P. Sharma, P. Kumar, P. Kumar, K. Gaskell, V.R. Satsangi, R. Shrivastav, S. Dass, Int. J. Hydrogen Energy 36 (2011) 5236–5245.
[36] L. Balakrishnan, S.G. Raj, S. Meher, K. Asokan, Z. Alex, Appl. Phys. A 119 (2015) 1541–1553.
[37] F.A. Mir, K.M. Batoo, Appl. Phys. A 122 (1–7) (2016) 418.
[38] R. Butté, L. Lahourcade, T.K. Uždavinys, G. Callsen, M. Mensi, M. Glauser, G. Rossbach, D. Martin, J. Carlin, S. Marcinkevičius, N. Grandjean, M. Mensi, M. Glauser, G. Rossbach, D. Martin, Appl. Phys. Lett. 112 (2018) (032106) 1–(032106)5.
[39] M. Beauvy, C. Dalmasso, C. Thiriet-dodane 242 (2006) 557–561.
[40] Y.S. Chaudhary, S.A. Khan, R. Shrivastav, V.R. Satsangi, S. Prakash, U.K. Tiwari, D.K. Avasthi, N. Goswami, S. Dass, Thin Solid Films 492 (2005) 332–336.
[41] P. Kumar, P. Sharma, A. Solanki, A. Tripathi, D. Deva, R. Shrivastav, S. Dass, V.R. Satsangi, Int. J. Hydrogen Energy 37 (2012) 3626–3632.
[42] P. Sharma, R. Singhal, R. Vishnoi, R. Kaushik, M.K. Banerjee, D.K. Avasthi, V. Ganesan, Vaccum 123 (2016) 35–41.
[43] N. Bajwa, A. Ingale, D.K. Avasthi, R. Kumar, A. Tripathi, K. Dharamvir, V.K. Jindal, J. Appl. Phys. 104 (2008) 1–13, 054306.
[44] M. Rao, K. Ravindranadh, A. Kasturi, M. Shekhawat, Res. J. Recent Sci. 2 (2013) 67–73.
[45] D. Carlos, V. Lavayen, C.O. Dwyer, J. Solid State Chem. 183 (2010) 1595–1603.
[46] A. Klinbumrung, T. Thongtem, S. Thongtem, J. Nanomater. 40 (2012) 1–5.
[47] G. Nazri, C. Julien, Solid State Ionics 56 (1992) 376–382.
[48] O. Lupan, V. Trofim, V. Cretu, I. Stamov, N.N. Syrbu, I. Tiginyanu, Y.K. Mishra, R. Adelung, J. Phys. D Appl. Phys. 47 (2014).
[49] S.K.S. Patel, K. Dewangan, S.K. Srivastav, N.K. Verma, P. Jena, A.K. Singh, N.S. Gajbhiye, Adv. Mater. Lett. 9 (2018) 585–589.
[50] A. Guru Sampath Kumar, T. Sofi Sarmash, L. Obulapathi, D. Jhansi Rani, T. Subba Rao, K. Asokan, Thin Solid Films 605 (2016) 102–107.
[51] R. Kumaravel, K. Ramamurthi, I. Sulania, K. Asokan, D. Kanjilal, D.K. Avasti, P.K. Kulria, Radiat. Phys. Chem. 80 (2011) 435–439.
[52] V. Naundorf, Int. J. Mod. Phys. B 6 (1992) 2925–2986.
[53] A. Axelevitch, B. Gorenstein, G. Golan, Phys. Procedia 32 (2012) 1–13.
[54] Y.S. Chaudhary, S.A. Khan, R. Shrivastav, Nucl. Instrum. Methods Phys. Res. B 225 (2004) 291–296.
[55] H. Thakur, S. Gautam, P. Thakur, K.K. Sharma, A.P. Singh, Y. Kumar, R. Kumar, K.H. Chae, J. Korean Phys. Soc. 61 (2011) 1609–1614.
[56] D. Allan Bromley, Treatise on Heavy-Ion Science, Springer Berlin Heidelberg, Newyork, 1985.
[57] S. Chandramohan, R. Sathyamoorthy, P. Sudhagar, D. Kanjilal, Nucl. Instrum. Methods Phys. Res. B 254 (2007) 236–242.
[58] H. Demiryont, J.R. Sites, K. Geib, Appl. Opt. 24 (2000) 490–495.
[59] M. Kovendhan, D.P. Joseph, P. Manimuthu, S. Ganesan, S. Sambasivam, P. Maruthamuthu, S.A. Suthanthiraraj, C. Venkateswaran, R. Mohan, Trans. Indian Inst. Met. 64 (2011) 185–188.
[60] V. Gokulakrishnan, S. Parthiban, E. Elangovan, K. Jeganathan, D. Kanjilal, K. Asokan, R. Martins, E. Fortunato, K. Ramamurthi, Radiat. Phys. Chem. 81 (2012) 589–593.
[61] P. Sharma, M. Vashistha, I.P. Jain, Opt. Mater. 27 (2004) 395–398.
[62] M.S. Kamboj, G. Kaur, R. Thangaraj, D. Avasthi, J. Phys. D Appl. Phys. 35 (2002) 477–479.
[63] S. Rani, N.K. Puri, S.C. Roy, M.C. Bhatnagar, D. Kanjilal, Nucl. Instrum. Methods Phys. Res. B 266 (2008) 1987–1992.
[64] N. Desai, V. Kondalkar, R. Mane, C. Hong, P. Bhosale, J. Nanomed. Nanotechnol. 6 (338) (2015) 1–7.
[65] X.W. Lou, H.C. Zeng, Chem. Mater. 14 (2002) 4781–4789.
[66] S. Bai, S. Chen, L. Chen, K. Zhang, R. Luo, D. Li, C. Chiun, Sensor. Actuator. B 174 (2012) 51–58.
[67] H.S. Zhang, J.L. Endrino, A. Anders, Appl. Surf. Sci. 255 (2008) 2551–2556.
[68] D.S. Rana, D.K. Chaturvedi, J.K. Quamara, Optoelectron. Adv. Mater. – RAPID Commun. 3 (2009) 737–743.
[69] S.G. Mayr, R.S. Averback, Phys. Rev. Lett. 87 (1–4) (2001) 196106.
[70] A.E. Volkov, Nucl. Instrum. Methods Phys. Res. B 193 (2016) 381–390.
[71] H. Thomas, S. Thomas, R. V Ramanujan, D.K. Avasthi, I.A.A. Omari, S. Al-harthi, M.R. Anantharaman, Nucl. Instrum. Methods Phys. Res. B 287 (2012) 85–90.
[72] S. Hemon, F. Gourbilleau, E. Paumier, E. Dooryhee, Nucl. Instrum. Methods Phys. Res. B 122 (1997) 526–529.
[73] A. Berthelot, S. Hémon, F. Gourbilleau, C. Dufour, B. Domengès, Philos. Mag. A 80 (2009) 2257–2281.
[74] D. Choi, Microelectron. Eng. 122 (2014) 5–8.
[75] T. Sun, B. Yao, A.P. Warren, K. Barmak, M.F. Toney, R.E. Peale, K.R. Coffey, Phys. Rev. B 81 (2010) 1–12.
[76] A.F. Mayadas, M. Shatzkes, Phys. Rev. B 1 (4) (1970) 1382–1389.
[77] P.M.R. Kumar, C.S. Kartha, K.P. Vijayakumar, F. Singh, D.K. Avasthi, P.M.R. Kumar, C.S. Kartha, K.P. Vijayakumar, J. Appl. Phys. 97 (2005) (013509) 1–(013509)6.
[78] M. Vasilopoulou, D.G. Georgiadou, L.C. Palilis, P. Argitis, S. Kennou, L. Sygellou, N. Konofaos, A. Iliadis, I. Kostis, G. Papadimitropoulos, D. Davazoglou, Microelectron. Eng. 90 (2012) 59–61.
[79] P.C. Srivastava, V. Ganesan, O.P. Sinha, Nucl. Instrum. Methods Phys. Res. B 222 (2004) 491–496.
[80] S. Kumar, A.K. Mahapatro, P. Mishra, Appl. Surf. Sci. 462 (2018) 815–821.